PHYSICAL REVIEW B, VOLUME 63, 024424

Disorder-induced orbital ordering in $L_{0.7}M_{0.3}MnO_3$ perovskites

Lide M. Rodríguez-Martínez* and J. Paul Attfield†
Department of Chemistry, University of Cambridge, Lensfield Road, Cambridge CB2 1EW, United Kingdom
and Interdisciplinary Research Centre in Superconductivity, University of Cambridge, Madingley Road,
Cambridge CB3 0HE, United Kingdom

(Received 10 July 2000; published 20 December 2000)

A series of eight $AMnO_3$ perovskites in which the A-cation sites are occupied by a distribution of 70% trivalent lanthanide and 30% divalent Ca, Sr, or Ba ions has been prepared. These all have a mean A-cation radius of 1.20 Å, but different values of the size variance σ^2. All of the samples show resistive and magnetic transitions from a ferromagnetic metallic to a paramagnetic insulating phase. An abrupt change from orbital disorder to order (cooperative Jahn–Teller distortions) in the insulating regime at $\sigma^2 \approx 0.005$ Å^2 is evidenced by anomalies in the unit cell parameters and conductivity and magnetization data. The dependence of the metal-insulator transition temperature upon A-cation distribution in these and other 30% doped compositions are compared against a simple model and displayed in a general phase diagram.

DOI: 10.1103/PhysRevB.63.024424 PACS number(s): 75.30.Kz, 71.30.+h, 71.70.Ej, 72.80.Ga

INTRODUCTION

The discovery of colossal magnetoresistances (CMR) at the ferromagnetic metal (FM) to paramagnetic insulator (PI) transition in $AMnO_3$ manganite perovskites has resulted in the study of materials with many different cation mixtures at the A perovskite sites.[1–4] In general, $A = L_{1-x}M_x$ where L is one or more trivalent lanthanide cations and M is divalent Ca, Sr or Ba. In early studies of the $A = La_{1-x}Ca_x$ and $La_{1-x}Sr_x$ systems, changes in physical property were related to the changing hole doping level x. Recent work has shown that physical properties can vary even at a constant value of x, a notable example is the $A = (La_{1-y}Pr_y)_{0.7}Ca_{0.3}$ system which changes from a low temperature FM state at $y = 0$ to a charge ordered antiferromagnetic insulator (COAFI) at $y = 1$. Phase coexistence around the $y \approx 0.3$ boundary between the two states is responsible for very large CMR effects.[5]

The simplest approach to account for variations of physical property with A site composition is to consider a quasirandom distribution of hard sphere cations over the A type sites. This has traditionally been parameterized through the average A cation radius $\langle r_A \rangle$, often expressed as the Goldschmidt tolerance factor t:

$$t = \frac{\langle r_A \rangle + r_O}{\sqrt{2}(r_{Mn} + r_O)}, \tag{1}$$

where r_{Mn} and r_o are the manganese and oxide ion radii, respectively. A strong $\langle r_A \rangle$ dependence of the FM to PI transition temperature T_m was evidenced for selected manganites,[1] but it was subsequently shown that a general description requires the use of an additional parameter, the A-cation size variance, $\sigma^2 = \langle r_A^2 \rangle - \langle r_A \rangle^2$.[6] At a constant x ($=0.3$) and $\langle r_A \rangle$, T_m shows a strong linear decrease with σ^2. Neutron diffraction studies have shown that this suppression of the FM phase is associated with an increasing spread of local Mn–O distances, supporting the view that the FM to PI transition is associated with localization of Jahn–Teller distortions of $Mn^{3+}O_6$ octahedra.[7,8] An analogous linear variation of the superconducting critical temperature with σ^2 has been reported in A_2CuO_4 materials.[9]

Perovskites such as the manganites also show a variety of superstructures arising from the ordering of different tilting or twisting modes of the octahedra. The transitions between the structural phases of manganites also vary with $\langle r_A \rangle$ and with σ^2.[8,10] A strong linear increase of structural transition temperature with σ^2 at constant $\langle r_A \rangle$ has been found for the tetragonal-orthorhombic transition in the layered A_2CuO_4 perovskites[11] and for the Curie temperature of doped $BaTiO_3$ ferroelectrics.[12]

In this study we investigate the intermediate size region of $L_{0.7}M_{0.3}MnO_3$ manganites between the previously investigated large $\langle r_A \rangle$ series, at which the FM–PI transition is observed, and the small $\langle r_A \rangle$ regime in which charge ordered states are formed at low temperatures.

EXPERIMENTAL

The eight compositions shown in Table I were chosen to have the same mean A-cation radius of $\langle r_A \rangle = 1.20$ Å, using standard nine-coordinate cation radii.[13] Polycrystalline samples were prepared under identical conditions by solid state reaction in air at 1350 °C and after the final heating they were quenched to room temperature. Iodometric titrations were carried out to determine the formal manganese oxidation state. Room temperature x-ray powder diffraction patterns were collected with a Stoe Stadi-*P* powder diffractometer using monochromatic Cu Kα_1 radiation and were Rietveld analyzed using the GSAS program[14] to extract the unit cell parameters. More highly resolved synchrotron powder data were collected for two of the samples on diffractometer BM16 at the ESRF, Grenoble at 300 K. These data were fitted by using a pseudo-Voigt peak shape function with an asymmetry correction to account for axial divergence at low angles,[15] giving the results shown in Table II.

Resistivity measurements on sintered polycrystalline bars were performed between 10 and 300 K using a standard four probe technique. Temperature dependent magnetizations were measured for powdered samples cooled in the measur-

TABLE I. Summary of chemical, structural, and physical data for the $L_{0.7}M_{0.3}$MnO$_3$ ($\langle r_A \rangle = 1.20$ Å) series.

Sample no.	A site composition	σ^2(Å^2)	Mn oxidation site	*Pnma* type	a (Å)	b (Å)	c (Å)	T_C (K)	T_m (K)
1	$La_{0.56}Pr_{0.14}Ca_{0.30}$	0.0003	3.34(4)	O″	5.4612(1)	7.7167(2)	5.4735(1)	215	222
2	$La_{0.20}Pr_{0.50}Sr_{0.10}Ca_{0.20}$	0.0016	3.32(4)	O″	5.4551(2)	7.7064(2)	5.4719(2)	197	202
3	$Pr_{0.44}Nd_{0.26}Sr_{0.19}Ca_{0.11}$	0.0029	3.34(4)	O″	5.4553(3)	7.7022(3)	5.4619(3)	190	194
4	$Pr_{0.15}Nd_{0.55}Sr_{0.23}Ca_{0.07}$	0.0036	3.34(4)	O″	5.4559(2)	7.7041(2)	5.4627(2)	180	191
5	$Nd_{0.70}Sr_{0.25}Ca_{0.25}$	0.0040	3.30(2)	O″	5.4564(5)	7.7017(2)	5.4574(5)	188	187
6	$Pr_{0.70}Ba_{0.07}Ca_{0.23}$	0.0055	3.32(2)	O′	5.4718(1)	7.7094(2)	5.4585(1)	108	87
7	$Sm_{0.11}Pr_{0.59}Ba_{0.09}Ca_{0.21}$	0.0074	3.34(6)	O′	5.4740(1)	7.7095(1)	5.4586(1)	90	88
8	$Nd_{0.70}Ba_{0.11}Ca_{0.19}$	0.0090	3.30(4)	O′	5.4694(2)	7.7020(2)	5.4543(2)	95	106

ing field of 500 Oe on a Quantum Design SQUID magnetometer.

RESULTS

Powder x-ray diffraction showed all eight samples to contain a single perovskite type phase, and the iodometric titration results in Table I demonstrate that there is no significant oxygen nonstoichiometry across the series. The x-ray powder diffraction patterns were Rietveld-fitted using an orthorhombic $\sqrt{2}a_p \times 2a_p \times \sqrt{2}a_p$ GdFeO$_3$ type model with *Pnma* symmetry[16] (a_p is the cubic perovskite cell parameter). Although only this single structure type is adopted across the series, the evolution of the cell parameters is not smooth, as evidenced by the peak positions in Fig. 1. The derived cell parameters in Table I show that the first five samples with $\sigma^2 < 0.005$ Å^2 have $c > a > b/\sqrt{2}$ whereas the last three samples have $a > c > b/\sqrt{2}$. These two regimes correspond to the O″ and O′ structures respectively.[17] The O′ phase is orbitally ordered and shows a long range, cooperative Jahn–Teller distortion of the lattice, as found in undoped LaMnO$_3$, although the magnitude of the average distortion is much reduced as Mn^{3+} is diluted with 30% Mn^{4+} which has no electronic distortion. The O″ structure is orbitally disordered, with Jahn–Teller distortions that may be locally correlated, but are not long range ordered through the lattice. Room temperature structure refinements of samples 5 and 6 were performed by fitting a single *Pnma* symmetry model to the ESRF synchrotron data, giving the results summarized in Table II.

TABLE II. Structural results (fitting factors, cell and atomic parameters, distances, and angles) for compositions 5 and 6 from Rietveld fits of a *Pnma* symmetry model [atomic positions: A (x,1/4,z); Mn (1/2,0,0); O(1) (x,1/4,z); O(2) (x,y,z)] to highly resolved synchrotron x-ray powder diffraction data collected at 300 K on BM16 using a wavelength of 0.3251 Å.

Sample		5 (O″ type)	6 (O′ type)
χ^2		3.63	2.20
R_{wp}(%)		8.67	7.78
a (Å)		5.46426(6)	5.470 18(4)
b (Å)		7.70971(6)	7.713 18(6)
c (Å)		5.46033(5)	5.461 81(4)
A	x	0.0260(6)	0.0260(6)
	z	−0.0053(2)	−0.0046(2)
	U_{iso}(Å^2)	0.00659(8)	0.010 23(8)
Mn	U_{iso}(Å^2)	0.0045(1)	0.0023(1)
O(1)	x	0.4877(8)	0.4867(8)
	z	0.071(2)	0.067(1)
	U_{iso}(Å^2)	0.010(2)	0.006(2)
O(2)	x	0.285(1)	0.2854(4)
	y	0.0319(6)	0.0343(5)
	z	−0.282(1)	−0.282(1)
	U_{iso}(Å^2)	0.014(1)	0.0091(9)
Mn–O(1)×2 (Å)		1.967(2)	1.965(1)
Mn–O(2)×2 (Å)		1.953(7)	1.955(6)
Mn–O(2)×2 (Å)		1.975(7)	1.983(5)
Mn–O(1)–Mn (°)		157.0(5)	157.7(4)
Mn–O(2)–Mn (°)		159.1(3)	157.9(2)

All of the samples show a ferromagnetic transition in the magnetization data (Fig. 2). The transitions in samples 1, 6, 7, and 8 are sharp but those in samples 2–5 are appreciably broadened. This may result from the near-coincidence of the magnetic and O″–O′ structural transitions leading to first order behavior. The Curie temperatures T_C (Table I) were

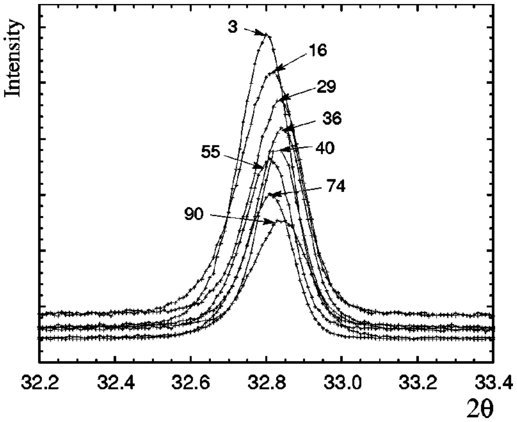

FIG. 1. Evolution of the (110) powder x-ray diffraction peak (indexed on the cubic perovskite cell) as the disorder σ^2 increases ($\sigma^2 \times 10^4$ Å^2 labeled). The peaks shift to higher 2θ with increasing σ^2, except for the displacement to lower 2θ between the $\sigma^2 = 0.0040$ and 0.0055 Å^2 samples, which evidences the change from O″ to O′ structure type.

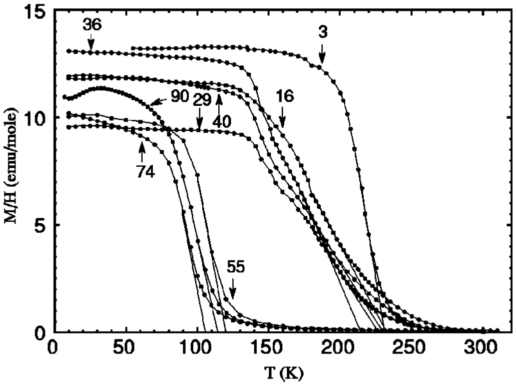

FIG. 2. Temperature dependence of the molar magnetization/field of samples with the $\sigma^2(\times 10^4\,\text{Å}^2)$ values labeled.

obtained from the minimum in $d(M/H)/dT$ curves.[1] At $\sigma^2 \approx 0.005\,\text{Å}^2$, between samples 5 and 6, there is a drop of 80 K in T_C coinciding with the change from O″- to O′-type orthorhombic structure.

Metal-to-insulator transitions are observed in the resistivity curves for all eight samples (Fig. 3) and the transition temperatures T_m were taken from the maxima. Again, there are two distinct groups on each side of the O″ to O′ structural change. Below $\sigma^2 \approx 0.005\,\text{Å}^2$, the samples have 290 K resistivities $\rho_{290\,\text{K}} \sim 0.1\,\Omega\,\text{cm}$ increasing to peak resistance $\sim 1\ \Omega\,\text{cm}$ at $T_m \sim 200\,\text{K}$. Samples with $\sigma^2 > 0.005\,\text{Å}^2$, have $\rho_{290\,\text{K}} \sim 0.3\,\Omega$ cm increasing to peak resistances $\sim 1500\ \Omega\,\text{cm}$ at $T_m \sim 100\,\text{K}$. As found for the previously studied $\langle r_{\text{A}} \rangle = 1.23\,\text{Å}$ (Ref. 6) and 1.26 Å (Refs. 18 and 19) series of $L_{0.7}M_{0.3}\text{MnO}_3$ perovskites, some of the samples with high σ^2 values show the presence of a shoulder, or for sample 8, a second resistivity peak.

Values of T_m, T_C, and $\rho_{290\,\text{K}}$, are plotted as a function of cation size disorder in Fig. 4. The metal-insulator and Curie temperatures are in good agreement. In the $\sigma^2 < 0.005\,\text{Å}^2$ region, a linear decrease with σ^2 is observed. Fitting the linear function $T_m = T_m^0 - p_1\sigma^2$ gives $T_m^0 = 221(4)\,\text{K}$ as an experimental estimate of the ideal insulator-metal transition temperature for $\langle r_{\text{A}} \rangle = 1.20\,\text{Å}$ $L_{0.7}M_{0.3}\text{MnO}_3$ perovskites if cation size disorder were not present, and $p_1 = 8900(1300)\,\text{K}\,\text{Å}^{-2}$ for the size variance dependence of the transition, $-dT_m/d\sigma^2$. The previously reported compositions $\text{Nd}_{0.7}\text{Sr}_{0.24}\text{Ca}_{0.06}\text{MnO}_3$ ($\langle r_{\text{A}} \rangle = 1.20\,\text{Å}$; $\sigma^2 = 0.0039\,\text{Å}^2$)[20] and $\text{Pr}_{0.7}\text{Sr}_{0.15}\text{Ca}_{0.15}\text{MnO}_3$ ($\langle r_{\text{A}} \rangle = 1.20\,\text{Å}$; $\sigma^2 = 0.0022\,\text{Å}^2$)[21] have T_m values of 185 and 205 K, respectively. These are in excellent agreement with our results and have been included in Fig. 4 (crossed squares) for comparison. The three samples with $\sigma^2 > 0.005\,\text{Å}^2$ do not show a clear trend of T_m with σ^2 and have $p_1 \approx 0$.

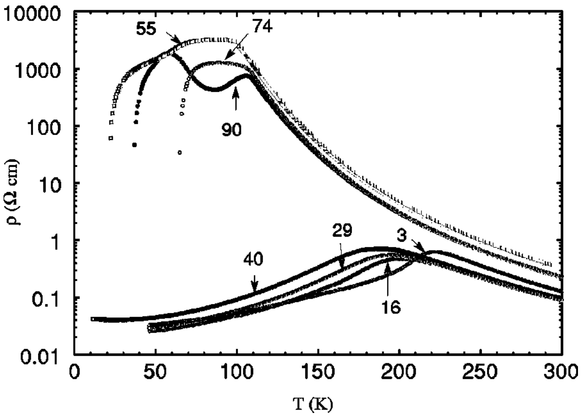

FIG. 3. Temperature dependence of resistivity of polycrystalline samples with the $\sigma^2(\times 10^4\,\text{Å}^2)$ values labeled. Data for sample $4(\sigma^2 = 0.0036\,\text{Å}^2)$ are omitted for clarity as they overlap heavily with those from samples 3 and 5.

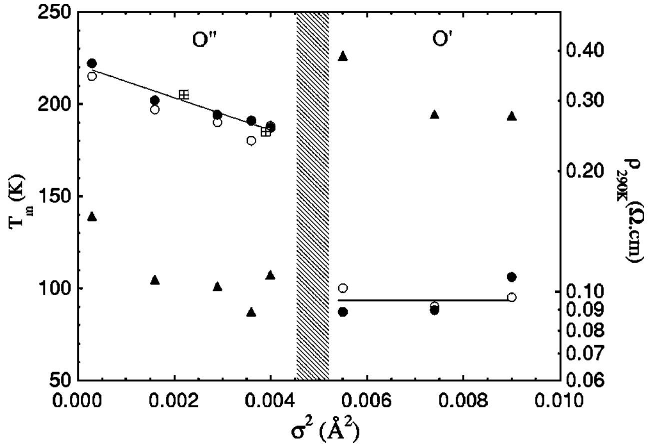

FIG. 4. Variation of the Curie (T_C, open circles) and metal-insulator (T_m, filled circles) transition temperatures and 290 K resistivity values (filled triangles) with σ^2 for the $\langle r_A \rangle = 1.20\,\text{Å}$ $L_{0.7}M_{0.3}\text{MnO}_3$ series. The crossed squares represent T_m data from the literature (see text). The approximate position of the border between O″ and O′ type structures is shown, and linear fits to T_m below and above this border are displayed.

DISCUSSION

The eight polycrystalline $\langle r_{\text{A}} \rangle = 1.20\,\text{Å}$ $L_{0.7}M_{0.3}\text{MnO}_3$ samples are homogeneous by x-ray diffraction and oxygen stoichiometric by iodometric titrations, and a detailed analytical electron microscopy study on similar samples prepared under the same conditions[7] has shown A-site compositions to be within ±3% of the nominal composition. However, in this and previous studies of polycrystalline manganites,[22,23] a broadening or splitting of the resistive transition is observed for high σ^2 samples. There is no evidence that this arises from chemical inhomogeneities. Maignan *et al.*[23] showed that the resistivity curves of $\text{Nd}_{0.7}\text{Ba}_{0.3}\text{MnO}_3$ single crystals and polycrystalline materials differ in appearance, with a second maximum below T_C only for the polycrystalline samples. They explained this observation on the basis of grain boundary effects, previously reported by Ju *et al.*[24] who related large strains at the grain boundary to the presence of large size differences between L^{3+} and M^{2+} cations. However, Shimura *et al.*[25] suggested that the double resistivity peaks in similar manganites are intrinsic to the bulk phase and Sun *et al.*[26] attributed this behavior to an inhomogeneous oxygen content. The most disordered sample of our series, sample 8 with σ^2

$=0.0090\,\text{Å}^2$, shows two resistivity peaks, at 106 and 58 K. The former peak is close to the ferromagnetic T_C of 95 K, and supports the view that the lower temperature peak results from the metallization of the grain boundary regions on cooling. The divergence between the bulk and grain boundary resistive transitions with σ^2 shows that the latter transition is the more sensitive to A-cation disorder effects.

A sharp discontinuity in the structural, conducting, and magnetic properties is seen at $\sigma^2 \approx 0.005\,\text{Å}^2$, between samples 5 and 6. Comparison of the cell parameters with those in other manganites shows that the transition is from an orbitally disordered $\text{O}''(c>a)$ to an orbitally ordered $\text{O}'(c<a)$ orthorhombic structure.[17] A similar transition from O″ to O′ type is found as the average ionic radius decreases in the $\text{Nd}_{0.7}\text{M}_{0.3}\text{MnO}_3$ series.[27,28] However, it is not clear whether the O″ to O′ transition occurs exactly at $a=c$, as the synchrotron refinement of O″-type sample 5 gives $a>c$. The refined structures of O″-type sample 5 and O′-type sample 6 (Table II) are consistent with orbital ordering in the latter sample, as the Mn–O(2′) bonds are significantly longer than the other four distances. However, the experimental uncertainties in the Mn–O distances are relatively large, and the results for sample 5 may be ambiguous as it is close to the O″–O′ border. Further neutron diffraction studies will be needed to ascertain the changes in crystal structure that accompany the transition in this series of samples.

It is notable that orbital *order* in the MnO_3 network is induced by increasing the size *disorder* (σ^2) at the A sites in this series of AMnO_3 perovskites. This is perhaps counterintuitive, and suggests that σ^2 should be viewed as a measure of the softness of the A-site environment in allowing the MnO_3 network to distort into the orbitally ordered arrangement. The same effect is observed for the structural transitions in doped La_2CuO_4 superconductors[11] and doped BaTiO_3 ferroelectrics.[12]

The abrupt fall in the FM to PI transition from 190 to 100 K at the orbital ordering boundary shows how strongly the electronic transport and magnetic order are linked to the Jahn–Teller distortions associated with the Mn^{3+} states. Neutron diffraction studies have shown that the metal to insulator transition is accompanied by a change from dynamic to static Jahn–Teller distortions.[29] This supports models featuring a localization of Jahn–Teller polarons at the transition.[30] The present results show that cooperative order of the distortions in the insulating (semiconducting) state reduces the carrier mobility leading to an increase by a factor of 3 in the 290 K resistivity and a reduction in the maximum temperature at which the metallic state is stable (i.e., T_m) by a factor of 2, compared to similar compositions in which orbital ordering does not occur in the insulating phase.

Comparing the variation of T_m in the $\langle r_\text{A}\rangle = 1.20\,\text{Å}$ series of $L_{0.7}M_{0.3}\text{MnO}_3$ perovskites with those from previous $\langle r_\text{A}\rangle = 1.23\,\text{Å}$ (Ref. 6) and 1.26 Å (Refs. 18 and 19) series enables trends with mean A-cation radius $\langle r_\text{A}\rangle$ and σ^2 to be seen. The slope $p_1 = (-dT_m/d\sigma^2)$ for the $\text{O}''-Pnma$ samples increases from $\sim 9000\ \text{K}\,\text{Å}^{-2}$ for $\langle r_\text{A}\rangle = 1.20\,\text{Å}$ to $\sim 20\,000\ \text{K}\,\text{Å}^{-2}$ for $\langle r_\text{A}\rangle = 1.23\,\text{Å}$. It was previously proposed that p_1 decreases with increasing $\langle r_\text{A}\rangle$ from comparisons of the 1.23 and 1.26 Å series, and similar work by Damay *et al.*[31] However, it is now clear that these larger $\langle r_\text{A}\rangle$ series have different perovskite superstructures, with orthorhombic *Imma* or rhombohedral $R\bar{3}c$ symmetry, and that p_1 is also sensitive to the superstructure type.[19] Hence, the inherent variation of p_1 with $\langle r_\text{A}\rangle$ can only be observed for a fixed perovskite superstructure. As $\langle r_\text{A}\rangle$ increases, p_1 increases within a superstructure type but decreases at the transition to other, higher symmetry superstructures. The variation of p_1 with $\langle r_\text{A}\rangle$ within the $\text{O}''-Pnma$ structure is in keeping with the previous suggestion[8] that σ^2 is important in creating local disortions (''preformed Jahn–Teller distortions'') or softening the lattice, both of which encourage polaron localization. Distortions of the perovskite structure increase as $\langle r_\text{A}\rangle$ decreases,[29] so that additional distortions due to the size variance at low $\langle r_\text{A}\rangle$ have a smaller influence on T_m than at high $\langle r_\text{A}\rangle$.

An empirical hard sphere ionic model was previously proposed to account for the variations of T_m with A-cation radii.[6,8,32] Local displacements of the oxygen atoms from the ideal positions that they would have in an undistorted cubic perovskite are given by $r_\text{A}^0 - r_\text{A}$ and these are assumed to give a strainlike energy which depresses T_m by an amount proportional to $\langle (r_\text{A}^0 - r_\text{A})^2\rangle$ ($\langle\rangle$ denotes an average). The equality

$$\langle (r_\text{A}^0 - r_\text{A})^2\rangle = \sigma^2 + (r_\text{A}^0 - \langle r_\text{A}\rangle)^2 \tag{2}$$

splits the total strain into incoherent and coherent terms, respectively, and leads to the expression

$$T_m = T_m^* - p_1\sigma^2 - p_2(r_\text{A}^0 - \langle r_\text{A}\rangle)^2, \tag{3}$$

where T_m^* is the ideal metal insulator transition temperature expected for a disorder-free ideal cubic perovskite with the same doping level and A-cation radius r_A^0 giving $t=1$ ($r_\text{A}^0 = 1.30\,\text{Å}$ for $x=0.3$). Equation (2) requires the coefficients p_1 and p_2 to be equal. In practice, p_1 and p_2 are not equal, but are of comparable magnitude ($\sim 10\,000$–$30\,000\ \text{K}\,\text{Å}^{-2}$). p_1 is dependent upon $\langle r_\text{A}\rangle$, as discussed above, but p_2 was found to be independent of σ^2. This may reflect changes in the perovskite superstructure type which are not taken into account in this first approximation model. The respective dependences of p_1 and p_2 on $\langle r_\text{A}\rangle$ and σ^2 remain to be determined fully.

The accuracy of the above description can be tested against a large amount of experimental data. Reported values of the metal-insulator transition T_m in 76 different $L_{0.7}M_{0.3}\text{MnO}_3$ perovskites are plotted against several functions of A-cation radius in Fig. 5. These data are taken from the present work, our previous results on $\langle r_\text{A}\rangle = 1.23$ (Ref. 6) and 1.26 Å (Refs. 18 and 19) series, and other reported results.[1,4,20,21,28] Figure 5(a) shows the variation of T_m with mean A-cation radius $\langle r_\text{A}\rangle$ [equivalent to the usual tolerance factor through Eq. (1)]. The upper boundary of the region occupied by the data is as reported previously for the $\langle r_\text{A}\rangle$ variation of T_m,[1] but it is clear that many compositions lie below this limit, as the effect of σ^2 is not included in this functional. Plotting T_m against the A-cation size variance σ^2

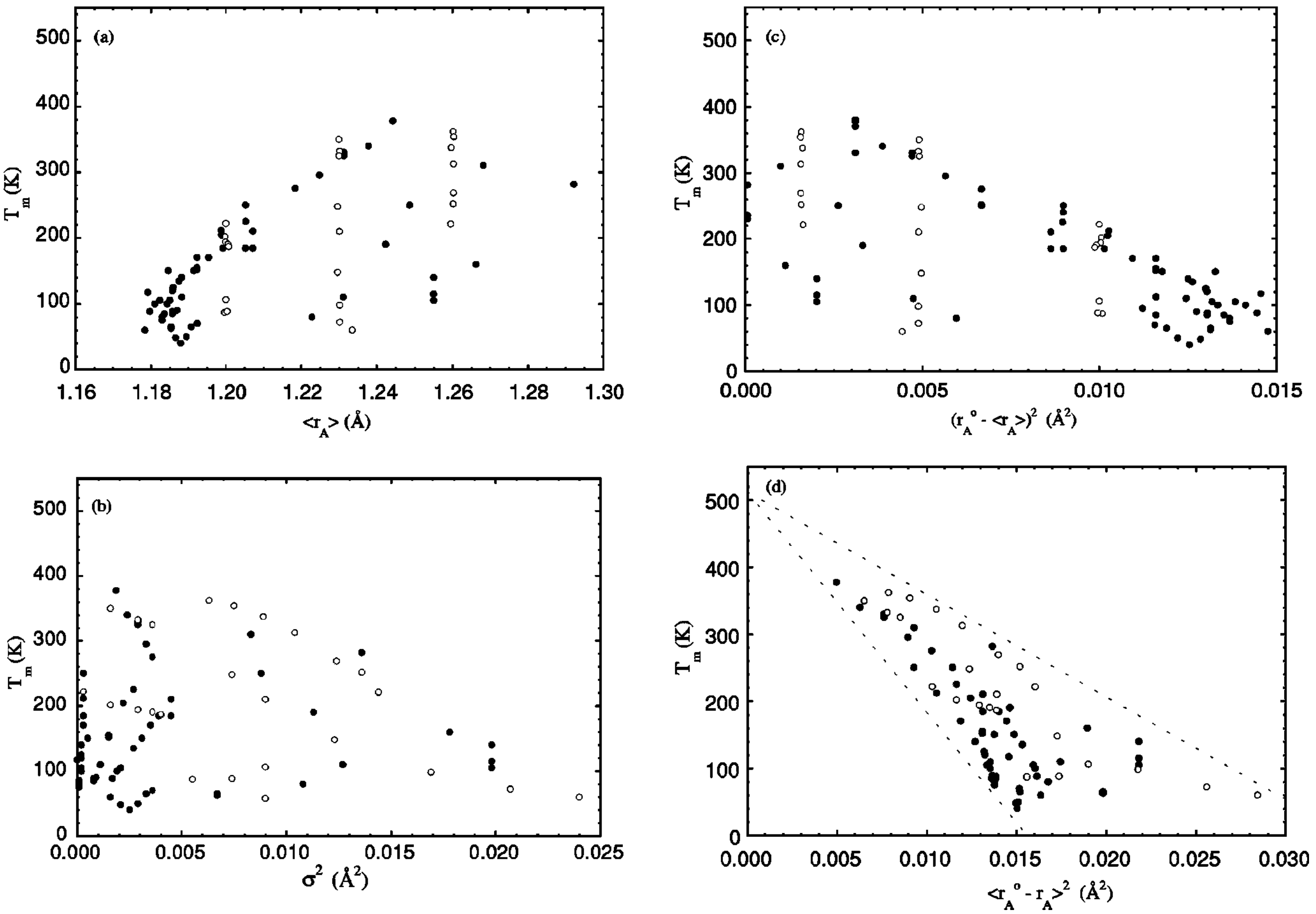

FIG. 5. Plots of experimental T_m values for $L_{0.7}M_{0.3}$MnO$_3$ compositions against: (a) average A-cation radius $\langle r_A \rangle$; (b) A-cation size variance σ^2; (c) $(r_A^0 - \langle r_A \rangle)^2$, [where r_A^0 is the ideal cubic perovskite A-cation radius, here $r_A^0 = 1.30$ Å]; and (d) the sum of σ^2 and $(r_A^0 - \langle r_A \rangle)^2$, which is $\langle (r_A^0 - r_A)^2 \rangle$. Filled and open circles correspond to data from other groups and from our publications, respectively (see text).

[Fig. 5(b)] also gives a large spread of data, as the effect of $\langle r_\mathrm{A} \rangle$ is not taken into account. Figure 5(c) uses the functional $(r_\mathrm{A}^0 - \langle r_\mathrm{A} \rangle)^2$, which is a quadratic function of mean radius. The similar distributions of T_m over the plots in Figs. 5(b) and 5(c), and the similar ranges of the two functionals in absolute Å^2 units corroborates the analogy between the effects of σ^2 and $(r_\mathrm{A}^0 - \langle r_\mathrm{A} \rangle)^2$ as incoherent and coherent strainlike effects. T_m is plotted against the total strain parameter $\langle (r_\mathrm{A}^0 - r_\mathrm{A})^2 \rangle$ in Fig. 5(d). This gives a much narrower distribution than the previous functionals as it allows for both the coherent and incoherent effects of the A-cation distribution. The data do not lie on a single line and tend to fan out as $\langle (r_\mathrm{A}^0 - r_\mathrm{A})^2 \rangle$ increases, reflecting discontinuities such as changes of perovskite superstructure type or orbital ordering which are known to change T_m. Extrapolating the upper and lower limits of the distribution back to $\langle (r_\mathrm{A}^0 - r_\mathrm{A})^2 \rangle = 0$, gives an estimate of 520 ± 20 K for T_m^* the metal-insulator transition in an ideal $L_{0.7}M_{0.3}$MnO$_3$ perovskite.

Figure 5 shows that $\langle (r_\mathrm{A}^0 - r_\mathrm{A})^2 \rangle$ is the best single functional based on ionic radii to account for the variation of T_m at a constant doping level, as it allows for both the coherent and incoherent effects of the A-cation distribution, whereas the traditional tolerance factor describes only the former effect. The ideal perovskite radius r_A^0 changes with doping level x (as r_Mn changes with oxidation state), so the normalized function $\langle (r_\mathrm{A}^0 - r_\mathrm{A})^2 \rangle / (r_\mathrm{A}^0)^2 = \langle (1 - r_\mathrm{A}/r_\mathrm{A}^0)^2 \rangle$ can be used as a dimensionless quantity in place of the tolerance factor to compare lattice effects in compositions with varying x.

Although $\langle (r_\mathrm{A}^0 - r_\mathrm{A})^2 \rangle$ provides a reasonable description, a more accurate description of chemical variations of property is obtained by treating $\langle r_\mathrm{A} \rangle$ and σ^2 as two independent parameters. In this approximation, the properties of all $L_{1-x}M_x$MnO$_3$ perovskites are described by the three variables x, $\langle r_\mathrm{A} \rangle$ and σ^2 so that all the chemical phase diagrams can be combined into a single diagram requiring four dimensions to display $T(x, \langle r_\mathrm{A} \rangle, \sigma^2)$. If x is fixed then this reduces to a three-dimensional plot which is plotted on the $\langle r_\mathrm{A} \rangle - \sigma^2$ plane for the $L_{0.7}M_{0.3}$MnO$_3$ perovskites in Fig. 6. (This plane was previously used by Damay *et al.*[31] to display various $L_{0.5}M_{0.5}$MnO$_3$ compositions.) All possible $L_{0.7}M_{0.3}$MnO$_3$ perovskites, for any number of L^{3+} and M^{2+} cations, lie in a finite region (the "chemical window") on this plot. The chemical window for $L =$ La–Sm and $M =$ Ca, Sr, Ba is shown on Fig. 6 and the positions of the binary $L_{0.7}M_{0.3}$ compositions that define the boundaries are marked. The

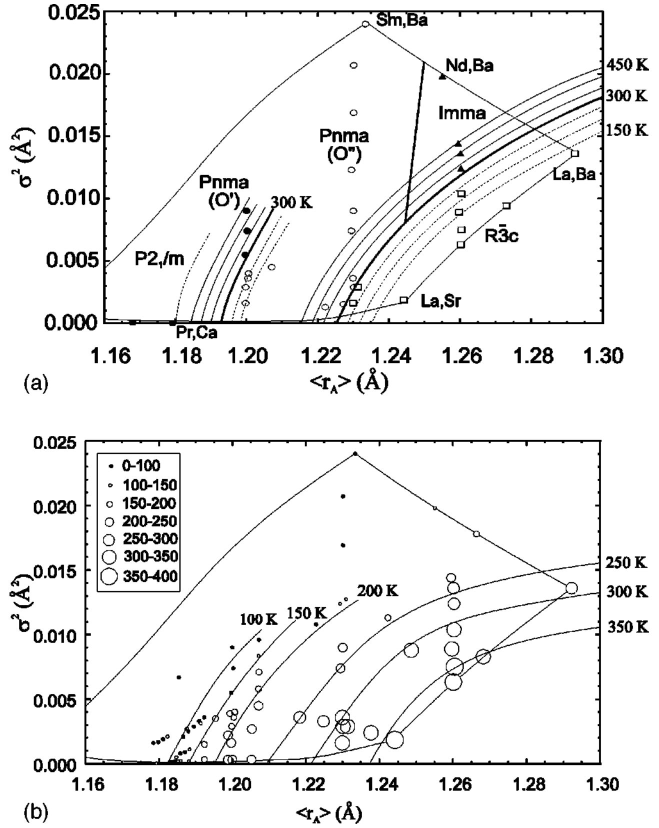

FIG. 6. Phase diagrams for $L_{0.7}M_{0.3}$MnO$_3$ plotted on the $\langle r_A\rangle - \sigma^2$ plane. The bounded region shows the chemical window within which all compositions for $L=$one or more of La, Pr, Nd, (Pm), Sm, and $M=$one or more of Ca, Sr, Ba lie. (a) The distribution of perovskite superstructures. Symbols indicate the labeled 300 K superstructures of samples from this work and Refs. 6, 18, 19, and selected binary $L_{0.7}M_{0.3}$ compositions. Isotherms are shown as solid lines for $T=300$ K and thin/broken lines for temperatures above/below 300 K. The positions of the $Pnma$–$Imma$ and $P2_1/m$–$Pnma$(O′) boundaries are not yet established and are shown as a single line. (b) Values of the metal-insulator transition (in 50 K intervals) and approximate isotherms are shown. The ideal $L_{0.7}M_{0.3}$MnO$_3$ perovskite (with $t=1$ and $\sigma^2=0$) lies at the bottom right corner of this plot and has estimated $T_m^*=520$ K.

L^{3+} cations all have radii at least 0.08 Å below the ideal A-cation radius of $r_A^0=1.30$ Å, so that the chemical window excludes the high $\langle r_A\rangle=r_A^0$ and $\sigma^2=0$ region around the ideal $L_{0.7}M_{0.3}$MnO$_3$ perovskite with $\langle r_A\rangle=r_A^0$ and $\sigma^2=0$.

All of the different superstructure types reported for $L_{0.7}M_{0.3}$MnO$_3$ perovskites are found to fall into different areas within the chemical window as shown in Fig. 6(a). The temperatures of the structural transitions between these superstructures have been determined in some cases, enabling thermal contours to be drawn, although the positions of others are still uncertain. At large $\langle r_A\rangle$ and σ^2 values, the materials show orthorhombic *Imma* symmetry (e.g., Nd$_{0.7}$Ba$_{0.3}$MnO$_3$),[33] whereas at large $\langle r_A\rangle$ and lower σ^2, the symmetry is rhombohedral $R\bar{3}c$ [e.g., La$_{0.7}$Ba$_{0.3}$MnO$_3$ (Ref. 29) and La$_{0.7}$Ba$_{0.18}$Sr$_{0.12}$MnO$_3$ (Ref. 10) at 300 K]. It is clear that the superstructure type depends upon σ^2 as well as $\langle r_A\rangle$ (or tolerance factor) and it is notable from Fig. 6(a) that the *Imma* type is only stabilized by having A-site cation mismatch with $\sigma^2>0.011$ Å^2. At intermediate values of $\langle r_A\rangle$, the orthorhombic $Pnma$ O″-superstructure is observed. All of the latter three superstructure types are found for both the low temperature FM and high temperature PI phases. Further decreasing $\langle r_A\rangle$ (e.g., in a series of compositions from La$_{0.7}$Ca$_{0.17}$Sr$_{0.13}$MnO$_3$ to Pr$_{0.7}$Ca$_{0.3}$MnO$_3$)[29] or increasing σ^2 (as in the present $\langle r_A\rangle=1.20$ Å series) leads to the O″ to O′ transition at which long range orbital ordering occurs in the high temperature PI phase. Charge ordered phases with monoclinic P2$_1$/m symmetry are observed at even lower $\langle r_A\rangle$. Further studies will be needed to locate the $Pnma$–$P2_1/m$ boundary more accurately and to find if additional charge ordered phases exist at low $\langle r_A\rangle$.

The variation of the metal-insulator transition within the chemical window for $L_{0.7}M_{0.3}$MnO$_3$ perovskites is shown in Fig. 6(b). The T_m isotherms are consistent with the maximum $T_m^*\sim 520$ K at the $\langle r_A\rangle=r_A^0=1.30$ Å, $\sigma^2=0$ position for an imaginary ideal perovskite, as above. The isotherms are quite evenly spaced in the 200–350 K range, but become more tightly packed in the 100–200 K interval as the transition from the orbitally disordered O″ to the orbitally ordered O′ insulator reduces T_m drastically, as shown in Fig. 4. Below $T_m=100$ K, charge ordering can also occur and two phase behavior is observed.[5]

In conclusion, this study demonstrates the usefulness of parameterizing the A-cation distribution of ABO$_3$ perovskites such as $L_{1-x}M_x$MnO$_3$ in terms of the doping level x, the mean A-cation radius $\langle r_A\rangle$ (equivalent to the traditional perovskite tolerance factor), and the A-cation size variance σ^2. In this case, fixing $x=0.3$ and $\langle r_A\rangle=1.20$ Å has enabled the σ^2 value at which long range orbital ordering occurs to be established, and a strong influence of orbital ordering on the metal-insulator transition and transport properties of the insulating phase is observed. Combining these data with T_m values from many other $x=0.3$ samples enables the $\langle r_A\rangle$ and σ^2 dependences to be seen, and the parameter $\langle(1-r_A/r_A^0)^2\rangle$ is proposed as the best single functional based on ionic radii, as it allows for both the coherent ($\langle r_A\rangle$) and incoherent (σ^2) strainlike effects of the A-cation distribution. This enables the maximum possible T_m for an idealized $L_{0.7}M_{0.3}$MnO$_3$ perovskite to be estimated as 520 K. $T(\langle r_A\rangle,\sigma^2)$ phase diagrams at constant x display the chemical window within which all $L_{1-x}M_x$MnO$_3$ compositions lie, and show the regions occupied by the various perovskite superstructure types and physical states, and the temperature dependences of the boundaries between them.

ACKNOWLEDGMENTS

The authors thank Dr. John Cooper and Steve Rycroft for assistance with resistivity measurements, Dr. Helmut Ehrenberg, Abbie McLaughlin, and Jon Wright, for performing data collection at the ESRF, and the British Council and Ministerio de Educacion y Cultura, Spain, for an Acciones Integradas award. L.M.R.M. acknowledges the Basque Government for funding.

*Present address: Departamentos de Química Inorgánica y de Mineralogía y Petrología, Universidad del País Vasco-Euskal Herriko Unibertsitatea, Apdo. 644, Bilbao 48080, Spain.

†Email address: jpa14@cam.ac.uk

[1] H. Y. Hwang, S. W. Cheong, P. G. Radaelli, M. Marezio, and B. Batlogg, Phys. Rev. Lett. **75**, 914 (1995).

[2] Z. Jirak, E. Pollert, A. F. Andersen, J. C. Grenier, and P. Hagenmuller, Eur. J. Solid State Inorg. Chem. **27**, 421 (1990).

[3] R. Mahesh, R. Mahendiran, A. K. Raychaudhuri, and C. N. R. Rao, J. Solid State Chem. **120**, 204 (1995).

[4] B. Raveau, A. Maignan, and V. Caignaert, J. Solid State Chem. **117**, 424 (1995).

[5] M. Uehara, S. Mori, C. H. Chen, and S.-W. Cheong, Nature (London) **399**, 560 (1999).

[6] L. M. Rodríguez-Martínez and J. P. Attfield, Phys. Rev. B **54**, R15622 (1996).

[7] L. M. Rodríguez-Martínez and J. P. Attfield, Chem. Mater. **11**, 1504 (1999).

[8] L. M. Rodríguez-Martínez and J. P. Attfield, Phys. Rev. B **58**, 2426 (1998).

[9] J. P. Attfield, A. L. Kharlanov, and J. A. McAllister, Nature (London) **394**, 157 (1998).

[10] P. G. Radaelli, M. Marezio, H. Y. Hwang, S.-W. Cheong, and B. Batlogg, J. Solid State Chem. **122**, 444 (1996).

[11] J. A. McAllister and J. P. Attfield, Phys. Rev. Lett. **83**, 3289 (1999).

[12] D. C. Sinclair and J. P. Attfield, Chem. Commun. (Cambridge) **16**, 1497 (1999).

[13] R. D. Shannon, Acta Crystallogr., Sect. A: Cryst. Phys., Diffr., Theor. Gen. Crystallogr. **32**, 751 (1976).

[14] A. C. Larson and R. B. von Dreele, *GSAS*: *General Structure Analysis System*, LANSCE, MS-H805, Los Alamos National Laboratory, Los Alamos, NM, 1994.

[15] L. W. Finger, D. E. Cox, and A. P. Jephcoat, J. Appl. Crystallogr. **27**, 892 (1994).

[16] S. Geller, J. Chem. Phys. **24**, 1236 (1956).

[17] P. M. Woodward, T. Vogt, D. E. Cox, A. Arulraj, C. N. R. Rao, P. Karen, and A. K. Cheetham, Chem. Mater. **10**, 3652 (1998).

[18] L. M. Rodríguez-Martínez, H. Ehrenberg, and J. P. Attfield, J. Solid State Chem. **148**, 20 (1999).

[19] L. M. Rodríguez-Martínez, H. Ehrenberg, and J. P. Attfield, Solid State Sciences **1**, 11 (2000).

[20] F. Millange, Ph.D. thesis, University of Caen, France (1998).

[21] J. Hejtmanek, Z. Jirak, D. Sedmidubsky, A. Maignan, Ch. Simon, V. Caignaert, C. Martin, and B. Raveau, Phys. Rev. B **54**, 11947 (1996).

[22] A. Barnabe, F. Millange, A. Maignan, M. Hervieu, B. Raveau, G. van Tendeloo, and P. Laffez, Chem. Mater. **10**, 252 (1998).

[23] A. Maignan, C. Martin, M. Hervieu, B. Raveau, and J. Hetmanek, Solid State Commun. **107**, 363 (1998).

[24] H. L. Ju and H. Sohn, Solid State Commun. **102**, 463 (1997).

[25] T. Shimura, T. Hayashi, Y. Inaguma, and M. Itoh, J. Solid State Chem. **124**, 250 (1996).

[26] J. R. Sun, G. H. Rao, Y. Z. Zhang, Appl. Phys. Lett. **72**, 3208 (1998).

[27] F. Millange, A. Maignan, V. Caignaert, Ch. Simon, and B. Raveau, Z. Phys. B **101**, 169 (1996).

[28] F. Millange, V. Caignaert, G. Mather, E. Suard, and B. Raveau, J. Solid State Chem. **127**, 131 (1996).

[29] P. G. Radaelli, G. Iannone, M. Marezio, H. Y. Hwang, S.-W. Cheong, J. D. Jorgensen, and D. N. Argyriou, Phys. Rev. B **56**, 8265 (1997).

[30] A. J. Millis, P. B. Littlewood, and B. I. Shraiman, Phys. Rev. Lett. **74**, 5144 (1995).

[31] F. Damay, C. Martin, A. Maignan, and B. Raveau, J. Appl. Phys. **82**, 6181 (1997).

[32] J. P. Attfield, Chem. Mater. **10**, 3239 (1998).

[33] F. Fauth, E. Suard, C. Martin, and F. Millange, Physica B **241**, 427 (1998).